Research Article | Vol. 26, No. 18 | 3 Sep 2018 | OPTICS EXPRESS 23705
Optics EXPRESS

Transitional Goos-Hänchen effect due to the topological phase transitions

WEIJIE WU,[1] WENSHUAI ZHANG,[1] SHIZHEN CHEN,[1] XIAOHUI LING,[1] WEIXING SHU,[2] HAILU LUO,[1,*] SHUANGCHUN WEN,[2] AND XIAOBO YIN[3]

[1]*Laboratory for spin photonics, School of Physics and Electronics, Hunan University, Changsha 410082,China*
[2]*Key Laboratory for Micro-/Nano-Optoelectronic Devices of Ministry of Education, School of Physics and Electronics, Hunan University, Changsha 410082, China*
[3]*Department of Mechanical Engineering, University of Colorado, Boulder, CO 80309, USA*
[*]*hailuluo@hnu.edu.cn*

Abstract: We examine the Goos-Hänchen (GH) effect for a Gaussian beam impinging on the surface of silicene whose topological phase transitions can be modulated by external electric field and/or irradiating circular polarized light. It is shown that both the spatial and angular shifts in the GH effect present a sharp jump due to the topological phase transitions. The transitional GH effect can be attributed to transitional optical conductivity, which relates to Berry curvature and Chern numbers. These results can be broadly extended to other two-dimensional atomic crystals in the graphene family. We believe that the transitional GH effect may offer a possible way to determine the Berry curvature, Chern numbers, and topological phase transition by a direct optical measurement.

1. Introduction

The topological phase transition has attracted great attention, not only for its fundamental scientific importance but also for its potential applications [1, 2]. Silicene is a monolayer of silicon atoms with buckled sublattices [3–6]. As a two-dimensional topological insulator, topological phase transitions in silicene can be modulated by external electric field and/or irradiating circular polarized light. Recently reported that graphene-like electronic band structure, supporting charge carriers behaving as massless Dirac fermions [7], exist in the silicene. The strong spin-orbit coupling provides a mass to Dirac electrons and favors an experimentally accessible Kane-Mele type quantum spin Hall effect [8, 9]. The interaction of external electric field and/or circularly polarized light with silicene makes Dirac mass controllable, which leads to topological phase transition. However, how to measure the topological phase transition in the experiment is still a challenging problem [10, 11].

The Goos-Hänchen (GH) effect [12] have exhibited remarkable potential for optical measurement and sensor [13, 14]. Recently, the GH effect on the surface of graphene has been investigated. [15–17]. It has been demonstrated that the beam shifts in GH effect are very sensitive to the quantized Hall conductivity of graphene in quantum Hall regime [18]. By incorporating the quantum weak measurement techniques [19–22], the GH shifts have been applied as pointer to detect the layers of graphene [23]. Therefore, we expect that GH effect would be sensitive to topological phase transitions in silicene. In a simple explanation, the GH effect is a position shift of the beam intensity distribution centroid relative to its geometrical optics position [24, 25]. The GH effect is attributed to the penetration of an evanescent field, and the time-averaged Poynting vector of the evanescent wave is directed along the interface. In fact, the angular and spatial GH effects are caused by the angular gradient of the amplitude and phase of complex reflection coefficients [26, 27]. The transitional GH effect manifests as a sharp jump

#334140 https://doi.org/10.1364/OE.26.023705
Journal © 2018 Received 1 Jun 2018; revised 3 Aug 2018; accepted 20 Aug 2018; published 29 Aug 2018

Optics EXPRESS

on the boundary of topological phase transitions, but this does not occur in the same regime of topological phase.

In this paper, the physical mechanism between different topological phases and transitional GH effect has been revealed through boundary conditions. Firstly, the optical conductivity and Dirac mass are used to depict topological phase diagram. Chern number and spin-Chern number have been calculated. Both optical conductivity and reflection coefficient have a very close relationship with Chern number. By regulating external electric field and/or irradiating circular polarized light, topological phase transition will occur. Then, the transitional GH effect appears. Since the transitional GH effect has a corresponding relationship with different topological states, we believe that this work provides a convenient scheme for directly optical measurement of the different topological features.

2. Topological phase transitions

Figure 1 illustrates that a Gaussian beam of frequency ω_0 impinges at an angle θ on a silicene-substrate system. A local coordinate system needs to be established to determine the position of the beam split. Since a static electric field E_z is applied along the z axis, an electrostatic potential $2lE_z$ among the two inequivalent sublattices of the monolayer can be generated. Furthermore, the properties of silicene can also be modified by irradiating circularly polarized light. The corresponding electromagnetic potential is given by $A(t) = (A_0 \sin \omega t, A_0 \cos \omega t)$, where $\omega \gg \omega_0$ is the frequency of circularly polarized light with $\omega < 0$ ($\omega > 0$) specifying left (right) circular polarization and A_0 is the amplitude. The incident beam generating GH effect can be written as $\tilde{E}_i \propto (\hat{\mathbf{x}}_i f_p + \hat{\mathbf{y}}_i f_s) \exp\left[-Z_R(k_{ix}^2 + k_{iy}^2)/2k_i\right]$ [28]. Here $Z_R = \pi w_0^2/\lambda$ is the Rayleigh range, k_i is the wave number, w_0 is the beam waist, the vectors $\hat{\mathbf{x}}, \hat{\mathbf{y}}$ represent the directions of parallel and perpendicular to the incidence plane, respectively. And the polarization of the beam is determined by the complex-valued unit vector $\hat{\mathbf{f}} = (f_p \hat{\mathbf{x}}_i + f_s \hat{\mathbf{y}}_i)/(|f_p|^2 + |f_s|^2)^{1/2}$.

Near the Fermi energy, the Rashba terms are ignored since the Rashba couplings is week. And these results still holds under the adiabatic condition [29, 30]. Therefore, the effective Dirac Hamiltonian can be written as [10, 11]

$$H_\eta = \hbar v_F(\eta k_x \tau_x + k_y \tau_y) + \lambda_{SO} \sigma_z \eta \tau_z - \ell E_z \tau_z - \Lambda \eta \tau_z. \tag{1}$$

Here $\sigma = (\sigma_x, \sigma_y, \sigma_z)$ and $\tau = (\tau_x, \tau_y, \tau_z)$ are the Pauli matrices of the spin and the sublattice pseudospin, respectively. $\eta = \pm 1$ is the valley index, v_F is the Fermi velocity, λ_{SO} is the effective spin-orbit (SO) coupling. ℓ is the buckled height, Λ is the coupling constant between the monolayer and the circularly polarized light. The first term is the Hamiltonian for Dirac electrons. The second term is the Kane-Mele spin-orbit coupling term. The third term is related to the perpendicular electric field E_z. And the last term is associated with the irradiating circular polarized light. By diagonalizing the Hamiltonian in Eq.(1), the band gap is given by $2|m_s^\eta|$ with the Dirac mass

$$m_s^\eta = \eta s \lambda_{SO} - \ell E_z - \eta \Lambda, \tag{2}$$

where $\Lambda = (eaA_0 v_F)^2 \hbar/\omega$, a is the lattice constant. That is to say, the Dirac mass can be controlled by applying electric field E_z and coherent laser beam.

In the momentum space, the gauge potential can be defined as $\mathcal{A}_i(\vec{k}) = i\langle\psi(\vec{k})|\frac{\partial}{\partial k_i}|\psi(\vec{k})\rangle$, where $\psi(\vec{k})$ is eigenvector of Hamiltonian, and vector $\mathcal{A}_i(\vec{k})$ is called the Berry connection. Then we may define the Berry curvature, $\mathcal{F}(\vec{k}) = \partial\mathcal{A}_y(\vec{k})/(\partial k_x) - \partial\mathcal{A}_x(\vec{k})/(\partial k_y)$. And the Chern number is the integral of the Berry curvature $\mathcal{F}(\vec{k})$ over the first Brillouin zone. Each topological phase is indexed by the Chern number C and the Z_2 index. The Z_2 index is identical to the spin-Chern number C_s modulo 2, when the spin s is a good quantum number. It is determined uniquely by the Dirac mass and the valley index, that is, $C_s^\eta = \eta sgn(m_s^\eta)/2$ for the

Optics EXPRESS

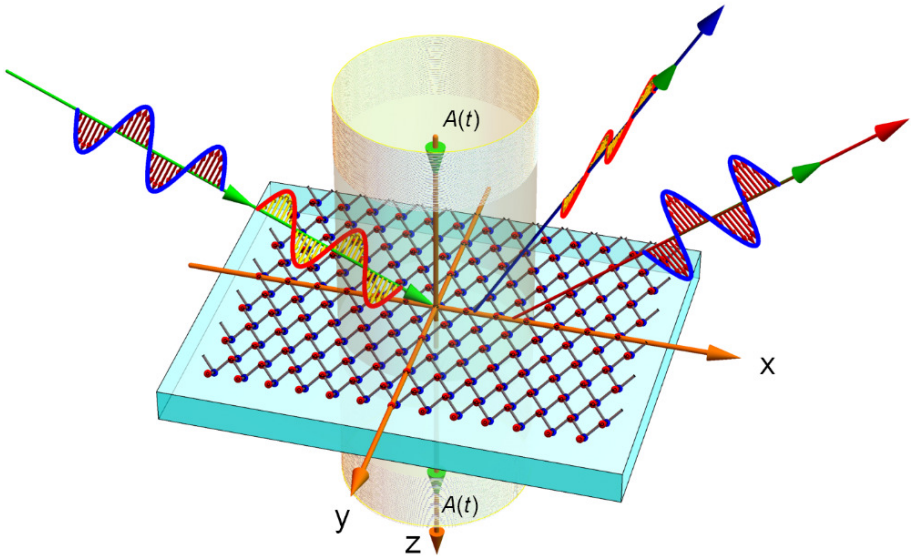

Fig. 1. Schematic representation of the wave reflection at a freestanding silicene sheet. The freestanding silicene is subjected to a static electric field E_z and a circularly polarized lasers. The lattice constant and staggering length values are $a = 3.86$, and $\ell = 0.23$, and the effective spin-orbit coupling $\lambda_{SO} = 3.9$meV. For the freestanding silicene, we can choose the refractive index of the substrate as $n = 1$.

K_η valley. Then, the Chern and spin-Chern numbers are obtained by $C = \sum_{\eta=\pm}(C_+^\eta + C_-^\eta)$ and $C_s = \sum_{\eta=\pm}(C_+^\eta - C_-^\eta)/2$. Therefore, the topological number is (C, C_s), as shown in the Fig. 2(d).

Using the Kubo's formula [31, 32], the expressions for the longitudinal and transverse Hall conductivities with zero temperature can be written as [33, 34]

$$\begin{aligned}\frac{\tilde{\sigma}_{xx}^{\eta s}}{\sigma_0/2\pi} &= \frac{4\mu^2 - |m_s^\eta|^2}{2\hbar\mu\Omega}\Theta(2\mu - |m_s^\eta|) + \left(1 - \frac{|m_s^\eta|^2}{\hbar^2\Omega^2}\right)tan^{-1}\left(\frac{\hbar\Omega}{M}\right) + \frac{|m_s^\eta|^2}{\hbar\Omega M},\\ \frac{\tilde{\sigma}_{xy}^{\eta s}}{\sigma_0/2\pi} &= \frac{2\eta m_s^\eta}{\hbar\Omega}tan^{-1}\left(\frac{\hbar\Omega}{M}\right).\end{aligned} \tag{3}$$

Here, $\sigma_0 = e^2/4\hbar$, $\tilde{\sigma}_{xx}^{\eta s} = \tilde{\sigma}_{yy}^{\eta s}$, $\tilde{\sigma}_{xy}^{\eta s} = -\tilde{\sigma}_{yx}^{\eta s}$, $M = \max(|m_s^\eta|, 2|\mu|)$, T is temperature, μ is doping, and $\Omega = -i\omega + \Gamma$, where Γ is the scattering rate.

The reflected amplitudes are obtained by solving Maxwell's equations and imposing the appropriate boundary conditions [35, 36], that is, $\mathbf{E}_i + \mathbf{E}_r = \mathbf{E}_t$ and $\mathbf{H}_i + \mathbf{H}_r - \mathbf{H}_t = \mathbf{J}$. To calculate the reflection of an incoming beams plane-polarized in an arbitrary direction, we decompose the incoming field into its p and s components. Sequentially, the four Fresnel's reflection coefficients, r_{ij} for incoming i-polarized and outgoing j-polarized plane waves, are obtained [37–39],

$$\begin{aligned} r_{pp} &= \frac{\alpha_-\beta_+ + \sigma_{ps}\sigma_{sp}}{\alpha_+\beta_+ + \sigma_{ps}\sigma_{sp}}, \qquad r_{ss} = \frac{\alpha_+\beta_- - \sigma_{ps}\sigma_{sp}}{\alpha_+\beta_+ + \sigma_{ps}\sigma_{sp}},\\ r_{ps} &= -\frac{2}{Z_i}\frac{\sigma_{ps}}{\alpha_+\beta_+ + \sigma_{ps}\sigma_{sp}}, \qquad r_{sp} = \frac{2}{Z_i}\frac{\sigma_{sp}}{\alpha_+\beta_+ + \sigma_{ps}\sigma_{sp}}. \end{aligned} \tag{4}$$

Here, $\alpha_+ = \sigma_{pp}k_{iz}/k_i + k_{iz}k_t/(Z_t k_i k_{tz}) + 1/Z_i$, $\alpha_- = \sigma_{pp}k_{iz}/k_i + k_{iz}k_t/(Z_t k_i k_{tz}) - 1/Z_i$,

Optics EXPRESS

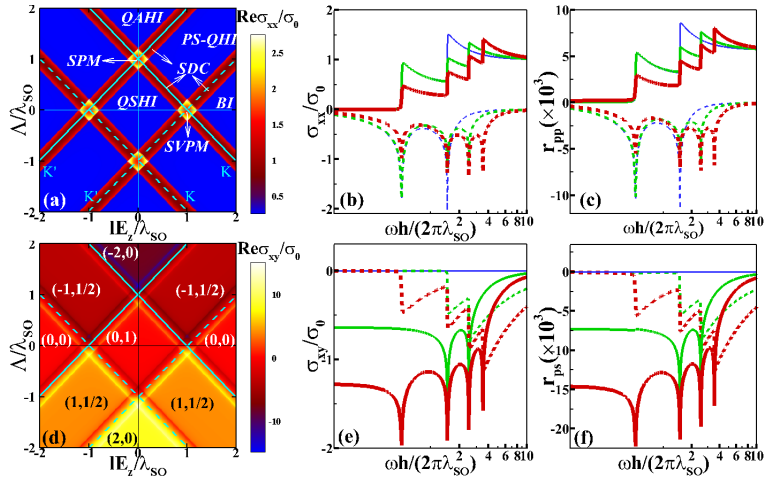

Fig. 2. Phase diagram of (a) longitudinal conductivity and (d) transverse Hall conductivity in the $(E_z, \Lambda)/\lambda_{SO}$ plane, and the Chern number and spin-Chern number (C, C_s) are also indicated. The solid line and the dashed line together outline the phase boundaries indexed by K_η, where the solid line represents the spin up ($s = +1$) and the dashed line represents the spin down ($s = -1$). (b) Longitudinal conductivity, (e) transverse Hall conductivity, (c) horizontally polarized reflection coefficient, and (f) cross-polarized reflection coefficient is a function of the photon energy of circularly polarized light in the states of QSHI, PS-QHI, and QAHI. The parameters are $\Lambda = 0\lambda_{SO}$(blue), $1\lambda_{SO}$(green), and $2\lambda_{SO}$(red), $E_z l = 0.5\lambda_{SO}$, $\hbar\Gamma = 0.002\lambda_{SO}$, $\mu = 0.1\lambda_{SO}$. And the solid (dashed) line represents the real (imaginary) part.

$\beta_+ = -\sigma_{ss}k_i/k_{iz} - k_i k_{tz}/(Z_t k_{iz} k_t) - 1/Z_i$, $\beta_- = \sigma_{ss}k_i/k_{iz} + k_i k_{tz}/(Z_t k_{iz} k_t) - 1/Z_i$, $Z_i = 1/\sqrt{\epsilon_i}$, and $Z_t = 1/\sqrt{\epsilon_t}$.

From Figs. 2(a) and 2(d), the Dirac mass plays an important role in the topological phase transition. That is, the phase boundaries appear when Dirac mass is zero. The occurrence of the topological phase transition is caused by the change of the sign of Dirac mass. For instance, if Λ is gradually increased from 0 and $E_z = 0$ remains unchanged, the entire system has undergone topological phase transition from quantum spin Hall insulator (QSHI) to spin-polarized metal (SPM) to quantum anomalous Hall insulator (QAHI). In other words, the band gap is also closed from the beginning of the open state and then reopening. In addition, when the topological numbers of the band insulator (BI) is $(0, 0)$, the QSHI being $(0, 1)$, the QAHI being $(-2, 0)$, and the photoinduced polarized-spin quantum Hall insulator (PS-QHI) being $(-1, 1/2)$, these states are insulators with the band gap open. All processes are adiabatically performed. Then, the SPM, spin-valley-polarized metal (SVPM), and single Dirac cone state appear at the intersection of different topological phase, and these gaps is closed.

From Figs. 2(b), 2(c), 2(e) and 2(f), the behavior of longitudinal conductivity, horizontally reflection coefficient, Hall conductivity, and cross-polarized reflection coefficient are illustrated as a function of the photon energy of circularly polarized light in the aforementioned topological phases. From Eq. (4), the optical conductivities have an impact on Fresnel's reflection coefficients and thus influence transitional GH effect. Next, note that cross-polarized reflection coefficient and transverse Hall conductivity are proportional to Chern number at low frequencies and small dissipation. The main reason is that the Hall conductivity can be reduced to be proportional to Chern number.

If $|m_s^\eta| > 2|\mu|$, we could get $M = |m_s^\eta|$. When $\hbar\Omega/|m_s^\eta|$ is small enough, the conductivity can be simplified to $\tilde{\sigma}_{xy}^{\eta s} = 2\sigma_0 \eta m_s^\eta \hbar\Omega/(2\pi\hbar\Omega|m_s^\eta|) = e^2 C_s^\eta/(2\pi\hbar)$. And the Hall conductivity is

Optics EXPRESS

$\sigma_{xy} = \sum_{\eta,s} \tilde{\sigma}_{xy}^{\eta s} = e^2 C/(2\pi\hbar)$, which is in good agreement with the description of Haldane [40]. Hence, the Hall conductivity can perfectly describe the topological phase diagram determined by Dirac mass. From Eq. (3), due to the relationship between the longitudinal conductivity and Dirac mass, the boundaries in phase diagram can still be described by longitudinal conductivity, but the different topological states cannot be depicted. In addition, the Hall conductivity is proportional to Chern number, the following two conditions need to be satisfied: (*i*) the absolute value of Dirac mass is greater than the absolute value of doping; (*ii*) $\hbar\Omega/|m_s^\eta|$ should be small enough. The Hall conductivity plays a important role in cross-polarized reflection coefficient. Considering the peaks caused by different photon energy, we find that the number of peaks of conductivity and the reflection coefficient is related to the Chern number as shown in Fig. 2.

3. Transitional Goos-Hänchen effect

To reveal the relation between the transitional GH effect and topological phase transitions, we give a derivation of the GH effect. Considering a incident Gaussian beam, the reflected light field can be obtained based on the boundary condition [18]

$$\begin{aligned}\mathbf{E}_r \propto & \exp\left(ik_i z_r - \frac{k_i}{2}\frac{x_r^2 + y_r^2}{Z_R + iz_r}\right) \\ \times & \left\{\hat{\mathbf{x}}_r\left[f_p r_{pp}\left(1 - \frac{ix_r}{Z_R + iz_r}\frac{\partial \ln r_{pp}}{\partial\theta_i}\right) + f_s r_{ps}\left(1 - \frac{ix_r}{Z_R + iz_r}\frac{\partial \ln r_{ps}}{\partial\theta_i}\right)\right]\right. \\ & \left. + \hat{\mathbf{y}}_r\left[f_s r_{ss}\left(1 - \frac{ix_r}{Z_R + iz_r}\frac{\partial \ln r_{ss}}{\partial\theta_i}\right) + f_p r_{sp}\left(1 - \frac{ix_r}{Z_R + iz_r}\frac{\partial \ln r_{ps}}{\partial\theta_i}\right)\right]\right\},\end{aligned} \tag{5}$$

where $f_p = a_p \in R$, $f_s = a_s \exp(i\eta)$.

By calculating the centroid of the reflected light field, the general GH effect expression is derived. That is,

$$D_{GH} = \frac{\int\int x_r I(x_r, y_r, z_r) dx_r dy_r}{\int\int I(x_r, y_r, z_r) dx_r dy_r}, \tag{6}$$

where I is beam intensity, and (x_r, y_r, z_r) is the reflected beam's coordinate frame. The beam intensity is closely linked to flux of the time averaged Poynting vector $I(x_r, y_r, z_r) \propto \bar{S} \cdot \hat{z}_r$. Then the Poynting vector related to the electromagnetic field can be obtained by $\bar{S} \propto \mathrm{Re}(\mathbf{E}_r \times \mathbf{H}_r^*)$.

After substituting Eq. (5) into Eq. (6), we get the following expression

$$D_{GH} = \frac{R_{pp}^2\varphi_{pp} + R_{sp}^2\varphi_{sp}}{k_i(R_{sp}^2 + R_{pp}^2)} - z_r\frac{R_{pp}^2\rho_{pp} + R_{sp}^2\rho_{sp}}{k_i(R_{sp}^2 + R_{pp}^2)Z_R}. \tag{7}$$

Here, $r_A = R_A \exp(i\phi_A)$, $A \in \{pp, ss, ps, sp\}$, $\rho_A = \mathrm{Re}(\partial \ln r_A/\partial\theta_i)$, and $\varphi_A = \mathrm{Im}(\partial \ln r_A/\partial\theta_i)$. The first term is the spatial shift, which does not changes with z_r. The second term is the angular deviation, and it is z_r-dependent [25].

We first consider the spatial shifts in GH effect. For p-polarization we have

$$\Delta_{GH}^P = \frac{R_{pp}^2\varphi_{pp} + R_{sp}^2\varphi_{sp}}{k_i(R_{pp}^2 + R_{sp}^2)}, \tag{8}$$

Similarly, if just consider the cross-polarized component, we obtain

$$\Delta_{GH}^{SP} = \frac{1}{k_i}\varphi_{sp}. \tag{9}$$

If s-polarization is considered, only the positions of s and p need to be interchanged. We have

$$\Delta_{GH}^S = \frac{R_{ss}^2\varphi_{ss} + R_{ps}^2\varphi_{ps}}{k_i(R_{ss}^2 + R_{ps}^2)}, \tag{10}$$

Optics EXPRESS

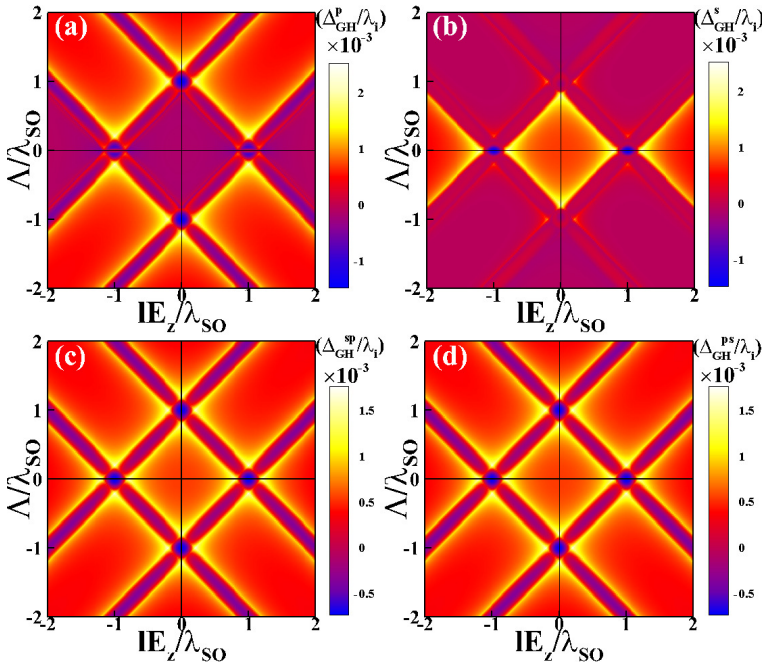

Fig. 3. Transitional spatial GH effect in the $(E_z, \Lambda)/\lambda_{SO}$ plane. The spatial shift, which is generated by (a) horizontally and (b) vertically polarized incident light, is a function of external electric field and coupling constants on the surface of silicene. The wavelength of incident light is $\lambda_i = hc/E$, incident angle $\theta_i = 60°$, $\hbar\omega = 0.1\lambda_{SO}$, and the beam waist is chosen as $w_0 = 1$mm. The (c) horizontally and (d) vertically polarized spatial shifts are modulated.

$$\Delta^{PS}_{GH} = \frac{1}{k_i}\varphi_{ps}. \tag{11}$$

From Eqs. (8)-(11), we find that the spatial shifts are related to the derivation of the phase of the complex Fresnel's reflection coefficients.

To confirms the topological phase transitions in silicene, the spatial shifts are plotted in Fig. 3. It is shown that the the original spatial shifts are very sensitive to the Chern numbers [Figs. 3(a) and 3(b)]. The magnitude of spatial shifts in the states of SPM, SVPM presents a sharp jump when a topological phase transition occurs. And the magnitude of spatial shifts in the single Dirac cone state, which is only one closed gap with a linear dispersion in K or K' points, has the same feature. The more clear jumping boundary in spatial shifts can be found if we only consider the beam shifts of the crossed components of reflected field [Figs. 3(c) and 3(d)].

We next consider the angular deviations in GH effect. For p-polarization, the expression of angular deviation is obtained as

$$\Theta^{P}_{GH} = -\frac{1}{k_i Z_R}\frac{R^2_{pp}\rho_{pp} + R^2_{sp}\rho_{sp}}{R^2_{sp} + R^2_{pp}}. \tag{12}$$

If we block the primary polarization with only the cross-polarized component being taken into consideration, we get

$$\Theta^{SP}_{GH} = -\frac{1}{k_i Z_R}\rho_{sp}. \tag{13}$$

Optics EXPRESS

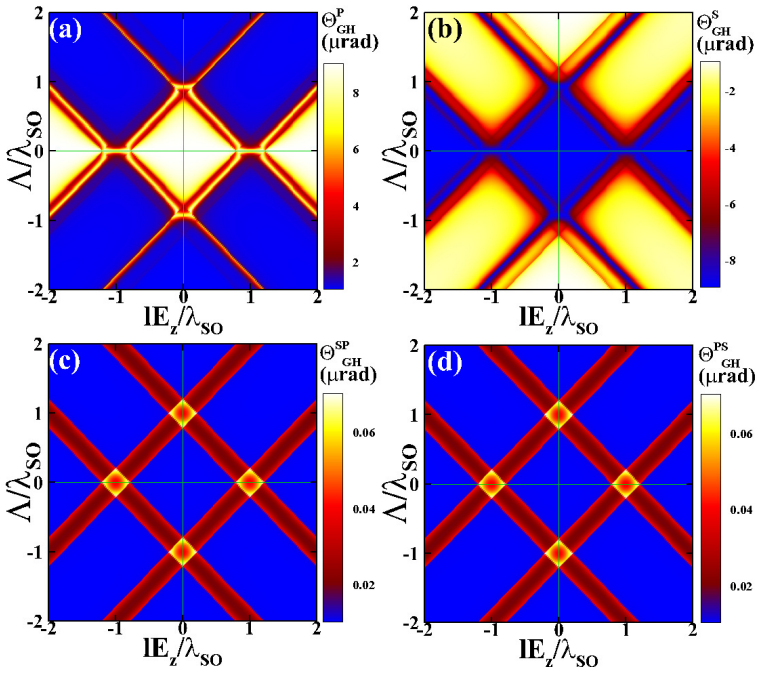

Fig. 4. Transitional angular GH effect in the $(E_z, \Lambda)/\lambda_{SO}$ plane. The angular deviation, which is generated by (a) horizontally and (b) vertically polarized incident light, is a function of external electric field and coupling constants on the surface of silicene. The (c) horizontally and (d) vertically polarized angular deviations are modulated. The parameters are the same as in Fig. 3.

If s-polarization is considered, only the positions of s and p need to be interchanged. So, we have

$$\Theta^{S}_{GH} = -\frac{1}{k_i Z_R}\frac{R^2_{ss}\rho_{ss} + R^2_{ps}\rho_{ps}}{R^2_{ps} + R^2_{ss}}, \tag{14}$$

$$\Theta^{PS}_{GH} = -\frac{1}{k_i Z_R}\rho_{ps}. \tag{15}$$

From Eqs. (12)-(15), we find that the angular deviations are related to the derivation of the amplitude of the complex Fresnel's reflection coefficients.

To further confirms the topological phase transitions in silicene, the angular deviations are plotted in Fig. 4. It is shown that the large angular deviations in the states of QSHI and BI are presented, where the Chern number is zero. For some states including QAHI and PS-QHI, the angular deviations are small where the Chern number is non-zero [Figs. 4(a) and 4(b)]. Hence, the GH effect provides a possible scheme to determine the Chern number. Similar to the case of spatial shifts, the clear jumping boundary in angular deviations can be found if we only consider the beam shifts of the crossed components of reflected field [Figs. 4(c) and 4(d)]. These interesting phenomenon is attributed to the Hall conductivity directly related to the topological phase transitions.

4. Conclusion

In conclusion, we have theoretically shown transitional GH effect due to the topological phase transition. By analyzing the Hamiltonian, we have demonstrated that the topological phase

Optics EXPRESS

diagram, which is described by GH effect, is consistent with the one described by Dirac mass. The topological number, including Chern number and spin-Chern number, can characterize different topological phases, and they are indicated in topological phase diagram. We have revealed that the transitional GH effect is sensitive to Chern number, topological phase transition. As a consequence, we believe that the experimental detection of topological phase transition by directly optical measurement is possible. Our method can be extended to entire graphene family including silicene, germanene, and stanene. Our results can also be extend to topological photonics [41, 42] due to the similar topological root.

Funding

National Natural Science Foundation of China (NSFC) (61835004); National Natural Science Foundation of China (NSFC) (11474089).

References

1. B. A. Bernevig, T. L. Hughes, and S.-C. Zhang, "Quantum spin Hall effect and topological phase transition in HgTe quantum wells," Science **314**(5806), 1757-1761 (2006).
2. S. Y. Xu, Y. Xia, L. A. Wray, S. Jia, F. Meier, J. H. Dil, J. Osterwalder, B. Slomski, A. Bansil, H. Lin, R. J. Cava, and M. Z. Hasan, "Topological Phase Transition and Texture Inversion in a Tunable Topological Insulator," Science **332**(6029), 560-564 (2011).
3. B. Lalmi, H. Oughaddou, H. Enriquez, A. Kara, S. Vizzini, B. Ealet, and B. Aufray, "Epitaxial growth of a silicene sheet," Appl. Phys. Lett. **97**(22), 223109 (2010).
4. C. C. Liu, W. X. Feng, and Y. G. Yao, "Quantum spin Hall effect in silicene and two-dimensional germanium," Phys. Rev. Lett. **107**(7), 076802 (2011).
5. L. Chen, C. C. Liu, B. Feng, X. He, P. Cheng, Z. Ding, S. Meng, Y. G. Yao, and K. H. Wu, "Evidence for Dirac fermions in a honeycomb lattice based on silicon," Phys. Rev. Lett. **109**(5), 056804 (2012).
6. P. Vogt, P. De Padova, C. Quaresima, J. Avila, E. Frantzeskakis, M. C. Asensio, A. Resta, B. Ealet, and G. L. Lay, "Silicene: compelling experimental evidence for graphenelike two-dimensional silicon," Phys. Rev. Lett. **108**(15), 155501 (2012).
7. S. Cahangirov, M. Topsakal, E. Akturk, H. Sahin, and S. Ciraci, "Two-and one-dimensional honeycomb structures of silicon and germanium," Phys. Rev. Lett. **102**(23), 236804 (2009).
8. C. L. Kane and E. J. Mele, "Quantum spin Hall effect in graphene," Phys. Rev. Lett. **95**(22), 226801 (2005).
9. C. L. Kane and E. J. Mele, "Z_2 Topological Order and the Quantum Spin Hall Effect," Phys. Rev. Lett. **95**(14), 146802 (2005).
10. M. Ezawa, "Valley-polarized metals and quantum anomalous Hall effect in silicene," Phys. Rev. Lett. **109**(5), 055502 (2012).
11. M. Ezawa, "Photoinduced topological phase transition and a single Dirac-cone state in silicene," Phys. Rev. Lett. **110**(2), 026603 (2013).
12. F. Goos and H. Hänchen, "Ein neuer und fundamentaler Versuch zur Totalreflexion," Ann. Phys. (Leipzig) **436**, 333-346 (1947).
13. X. Yin, L. Hesselink, Z. Liu, N. Fang, and X. Zhang, "Large positive and negative lateral optical beam displacements due to surface plasmon resonance," Appl. Phys. Lett. **85**(3), 372 (2004).
14. X. Yin and L. Hesselink, "Goos-Hänchen shift surface plasmon resonance sensor," Appl. Phys. Lett. **89**(26), 261108 (2006).
15. N. Hermosa, "Reflection beamshifts of visible light due to graphene," J. Opt. **18**(2), 025612 (2016).
16. X. Li, P. Wang, F. Xing, X. D. Chen, Z. B. Liu, and J. G. Tian, "Experimental observation of a giant Goos-Hänchen shift in graphene using a beam splitter scanning method," Opt. Lett. **39**(19), 5574-5577 (2014).
17. X. Zeng, M. Al-Amri, and M. Suhail Zubairy, "Tunable Goos-Hänchen shift from graphene ribbon array," Opt. Express **25**(20), 23579 (2017).
18. W. Wu, S. Chen, C. Mi, W. Zhang, H. Luo, and S. Wen, "Giant quantized Goos-Hänchen effect on the surface of graphene in the quantum Hall regime," Phys. Rev. A **96**(4), 043814 (2017).
19. Y. Aharonov, D. Z. Albert, and L. Vaidman, "How the result of a measurement of a component of the spin of a spin -1/2 particle can turn out to be 100," Phys. Rev. Lett. **60**(14), 1351-1354 (1988).
20. X. Zhou, Z. Xiao, H. Luo, and S. Wen, "Experimental observation of the spin Hall effect of light on a nanometal film via weak measurements," Phys. Rev. A **85**(4), 043809 (2012).
21. X. Zhou, X. Ling, H. Luo, and S. Wen, X. Zhou, X. Ling, H. Luo, and S. Wen, "Identifying graphene layers via spin Hall effect of light," Appl. Phys. Lett. Appl. Phys. Lett. **101**(25), 251602 (2012).
22. J. Dressel, M. Malik, F. M. Miatto, A. N. Jordan, and R. W. Boyd, "Colloquium: Understanding quantum weak values: Basics and applications," Rev. Mod. Phys. **86**(1), 307-316 (2014).

Optics EXPRESS

23. S. Chen, C. Mi, L. Cai, M. Liu, H. Luo, and S. Wen, "Observation of the Goos-Hänchen shift in graphene via weak measurements," Appl. Phys. Lett. **110**(3), 031105 (2017).
24. S. Grosche, A. Szameit, and M. Ornigotti, "Spatial Goos-Hänchen shift in photonic graphene," Phys. Rev. A **94**(6), 063831 (2016).
25. M. Merano, A. Aiello, M. P. Van Exter, and J. P. Woerdman, "Observing angular deviations in the specular reflection of a light beam," Nat. Photonics **3**(6), 337-340 (2009).
26. H. Schomerus and M. Hentschel, "Correcting ray optics at curved dielectric microresonator interfaces: phase-space unification of Fresnel filtering and the Goos-Hänchen shift," Phys. Rev. Lett. **96**(24), 243903 (2006).
27. K. Y. Bliokh and A. Aiello, "Goos-Hänchen and Imbert-Fedorov shifts: an overwiev," J. Opt. **15**(1), 014001 (2013).
28. A. Aiello and J. P. Woerdman, "Role of beam propagation in Goos-Hänchen and Imbert-Fedorov shifts," Opt. Lett. **33**(13), 1437 (2008).
29. D. N. Sheng, Z. Y. Weng, L. Sheng, and F. D. M. Haldane, "Quantum spin-Hall effect and topologically invariant Chern numbers," Phys. Rev. Lett. **97**(3), 036808 (2006).
30. E. Prodan, "Robustness of the spin-Chern number," Phys. Rev. B **80**(12), 125327 (2009).
31. R. Kubo, "Statistical-mechanical theory of irreversible processes. I. General theory and simple applications to magnetic and conduction problems," J. Phys. Soc. Jpn. **12**(6), 570-586 (1957).
32. L. Stille, C. J. Tabert, and E. J. Nicol, "Optical signatures of the tunable band gap and valley-spin coupling in silicene," Phys. Rev. B **86**(19), 195405 (2012).
33. W. J. M. Kort-Kamp, "Topological phase transitions in the photonic spin Hall effect," Phys. Rev. Lett. **119**(14), 147401 (2017).
34. P. Rodriguez-Lopez, W. J. M. Kort-Kamp, D. A. R. Dalvit, and L. M. Woods, "Casimir force phase transitions in the graphene family," Nat. Commun. **8**, 14699 (2017)
35. M. Merano, "Transverse electric surface mode in atomically thin boron-nitride," Opt. Lett. **41**(11), 2668-2671 (2016).
36. M. Merano, "Optical beam shifts in graphene and single-layer boron-nitride," Opt. Lett. **41**(24), 5780-5783 (2016).
37. M. Liu, L. Cai, S. Chen, Y. Liu, H. Luo, and S. Wen, "Strong spin-orbit interaction of light on the surface of atomically thin crystals," Phys. Rev. A **95**(6), 063827 (2017).
38. L. Cai, M. Liu, S. Chen, Y. Liu, W. Shu, H. Luo, and S. Wen, "Quantized photonic spin Hall effect in graphene," Phys. Rev. A **95**(1), 013809 (2017).
39. W. Zhang, W. Wu, S. Chen, J. Zhang, X. Ling, W. Shu, H. luo, and S. Wen, "Photonic spin Hall effect on the surface of anisotropic two-dimensional atomic crystals," Photonics Res. **6**(6), 511 (2018).
40. F. D. M. Haldane, "Nobel lecture: Topological quantum matter," Rev. Mod. Phys. **89**(4), 040502 (2017).
41. L. Lu, J. D. Joannopoulos, and M. Soljačić, "Topological photonics," Nat. Photonics **8**(11), 821-829 (2014).
42. B. Yang, Q. Guo, B. Tremain, R. Liu, L. E. Barr, Q. Yan, W. Gao, H. Liu, Y. Xiang, J. Chen, C. Fang, A. Hibbins, L. Lu, and S. Zhang, "Ideal Weyl points and helicoid surface states in artificial photonic crystal structures," Science **359**(6379), 1013-1016 (2018).